Interface characterization of B_4C-based multilayers by X-ray grazing-incidence reflectivity and diffuse scattering

Hui Jiang,[a]* Zhanshan Wang[b] and Jingtao Zhu[b]

[a]Shanghai Synchrotron Radiation Facility, Shanghai Institute of Applied Physics, Chinese Academy of Sciences, Zhangheng Road 239, Pudong District, Shanghai 201204, People's Republic of China, and [b]Institute of Precision Optical Engineering, Department of Physics, Tongji University, Shanghai 200092, People's Republic of China. E-mail: jianghui@sinap.ac.cn

B_4C-based multilayers have important applications for soft to hard X-rays. In this paper, X-ray grazing-incidence reflectivity and diffuse scattering, combining various analysis methods, were used to characterize the structure of B_4C-based multilayers including layer thickness, density, interfacial roughness, interdiffusion, correlation length, *etc*. Quantitative results for W/B_4C, Mo/B_4C and La/B_4C multilayers were compared. W/B_4C multilayers show the sharpest interfaces and most stable structures. The roughness replications of La/B_4C and Mo/B_4C multilayers are not strong, and oxidations and structure expansions are found in the aging process. This work provides guidance for future fabrication and characterization of B_4C-based multilayers.

Keywords: boron carbide; multilayer; X-ray reflectivity; diffuse scattering; interface; aging.

1. Introduction

Multilayer mirrors are artificial one-dimensional crystals with wide applications in the X-ray and extreme ultraviolet regime. For synchrotron radiation science they are considered key components for reflection (Windt *et al.*, 2002), polarization (Wang *et al.*, 2011), focusing (Mimura *et al.*, 2010) and monochromatization (Rack *et al.*, 2010). Compared with transmission focusing optics, they provide higher efficiency and realise nanofocusing more easily. Compared with a double-crystal monochromator, they provide more flux due to a wider bandpass and their large *d*-spacing extends their ranges to the soft X-ray region. Boron carbide (B_4C) based multilayers have valuable applications in synchronization radiation (Rack *et al.*, 2010), space observation (Joensen *et al.*, 1995), biological microscopy (Gutman, 1994), *etc*. The stable capping or barrier layer of B_4C multilayers (Bottger *et al.*, 2003) expands application opportunities.

Each layer in a multilayer mirror is very thin, typically several nanometers to less than 1 nm, and mirror performance depends on the quality of the layer interfaces. The most effective methods of characterizing multilayers are hard X-ray grazing-incidence reflectivity and diffuse scattering measurements. Detailed characterization can estimate defects introduced during fabrication, and offers feedback for improving the manufacture technology. Characterization also allows inspection of component quality in storage or during service to estimate their lifetime.

In this paper, various B_4C-based multilayers were fabricated and investigated by X-ray reflectivity and diffuse scattering techniques. Interfacial roughnesses, roughness correlations, interdiffusion, layer densities and their aging effects were characterized and compared systematically.

2. Experiment and method

2.1. Fabrication

All multilayer samples were deposited by DC magnetron sputtering on silicon substrates with a RMS roughness of $\sim$0.3 nm at room temperature. For W/B_4C multilayers the base vacuum was 1.2×10^{-4} Pa and the argon gas pressure (purity 99.999%) was 0.667 Pa. The sputtering powers for the W (purity 99.95%) and B_4C (purity 99.50%) targets were 20 W and 150 W, respectively. For Mo/B_4C and La/B_4C multilayers the base vacuum was 1×10^{-4} Pa and the argon gas pressure was 0.18 Pa. The sputtering powers for the Mo, La (purity 99.95%) and B_4C targets were 10 W, 10 W and 80 W, respectively. The distance between substrate and targets was 8 cm. All samples were measured using a high-resolution X-ray diffractometer (BEDE D1) at the Cu K_α line. The X-ray reflectivity measurement was run using only the second channel-cut crystal with a divergence angle of 0.007°, and the non-specular diffuse-scattering measurement was run in direct-beam mode to increase the X-ray intensity.

2.2. X-ray reflectivity and diffuse scattering

X-ray grazing-incidence reflectivity is an effective, simple and non-destructive technique for characterizing the structure parameters in a multilayer (Gibaud & Hazra, 2000). For periodic multilayers the behavior is described by a corrected Bragg equation with constant periodic thickness D, fractional thicknesses of absorber (scattering) layers d_a and spacer layers d_s, and complex refractive indices $n_a = 1 - \delta_a + i\beta_a$ and $n_s = 1 - \delta_s + i\beta_s$,

$$m\lambda = 2D \sin\theta \left[1 - \frac{2(d_a\delta_a + d_s\delta_s)}{\sin^2\theta} \right]^{1/2}, \qquad (1)$$

where m is the reflection order, λ is the wavelength and θ is the grazing-incidence angle. This equation relates the periodic thickness and the grazing-incidence angles. According to the positions of different sharp Bragg reflection maximums, based on the method of least squares, the periodic thickness can be calculated. The thickness ratio $\Gamma = d_a/D$ is related to the distribution of peak intensities. When $m\Gamma$ is a positive integer, the mth ($m = 1, 2, 3\ldots$) Bragg maximum disappears.

Another effective method of obtaining information about layer thickness is based on the Fourier transform. Parratt's recurrence formula (Parratt, 1954) can be kinetically approximated and the reflectivity is related to an auto-correlation function (ACF) (Bridou et al., 2006),

$$\mathrm{ACF}(z) = (2\pi)^{1/2} k_0^4 \sum_{i,j=1}^{N} \left(\delta\chi_i \delta\chi_j / \sigma_{ij} \right)$$
$$\times \exp\left[-(z - z_{ij})^2 / (2\sigma_{ij}^2) \right], \qquad (2)$$

where k_0 is the modulus of the incident wavevector, $\delta\chi$ is the polarizability change, $Z_{ij} = |Z_i - Z_j|$ is the distance between the jth and ith interfaces, and the interfacial width $\sigma_{ij}^2 = \sigma_i^2 + \sigma_j^2$. According to the positions and widths of the ACF maxima, the layer thickness and interfacial width can be obtained.

More accurate structure parameters need to be estimated by fitting the reflectivity curve. In order to realise good agreement between the experimental and theoretical curves of Parratt's model, global optimization (Wormington et al., 1999) can be used to search for the optimum simulated structure in a given constraint.

X-ray reflectivity is unable to distinguish between interfacial roughness and interdiffusion because both deteriorate the reflectivity in a similar way. X-ray diffuse scattering is one of the most direct techniques for determining interfacial roughnesses in a complicated multilayer structure. A distorted-wave Born approximation (DWBA) model (Holý et al., 1993) is suitable for slightly rough interfaces. The scattering potential is divided into a non-disturbed part and a disturbance. Interferences of reflected and transmitted waves have four types of interaction based on the dynamic scattering process (Stepanov et al., 1996). The whole diffuse scattering signal (Stoev & Sakurai, 1997) is represented by

$$I_{\mathrm{diff}} = I_0 \frac{\Delta\Omega}{2} \frac{A_s}{A_b} \sum_{j,k=1}^{N} \left| n_j^2 - n_{j+1}^2 \right|^2 \sum_{m,n=0}^{3} S_{j,k}^{mn}(q_x) \tilde{G}_j^m (\tilde{G}_k^n)$$
$$\times \exp\left(-\frac{1}{2} \left\{ \left(q_{z,j}^m \sigma_j \right)^2 + \left[\left(q_{z,k}^n \right)^* \sigma_k \right]^2 \right\} \right), \qquad (3)$$

where $\Delta\Omega$ is the detector acceptance angle, A_s/A_b is the area ratio of the radiation on the sample to the beam spot, G_j^m are the four mutual products of T_i (or R_i) and T_s (or R_s), and $S(q_x)$ is the structure factor

$$S_{j,k} = \int_0^{\infty} C_{j,k}(x) \cos(q_x x)\, \mathrm{d}x\, \exp\left(-|Z_j - Z_k|/\xi_\perp \right) \qquad (4)$$

where $\xi_\perp$ is the vertical correlation length (Pape et al., 1998) and $C(x)$ is the lateral correlation function which is based on the self-affine characteristic of the rough interface (Sinha et al., 1988),

$$C_{j,k}(x) = (1/2)\left[C_j(x) + C_k(x) \right],$$
$$C_j(x) = \sigma_j^2 \exp\left[-\left(x/\xi_\parallel \right)^{2h} \right], \qquad (5)$$

where $\xi_\parallel$ is the lateral correlation length and h is the fractal exponent.

The diffuse scattering signals are distributed around the reflection direction. Common scan methods include rocking curve scans (ω scan), offset scans, detector 2θ scans and full reciprocal-space scans. Rocking curve scans are performed by fixing the detector and scanning the incidence angle, whose track is parallel to the q_x direction. Owing to the proportional relationship between q_x and the roughness frequency, this method is very sensitive in determining roughness information. The method of scattering curve fitting is also based on global optimization to approach the real multilayer structure.

3. Result and discussion

Eight multilayers were measured using the X-ray grazing-incidence reflectivity technique including three W/B_4C, three Mo/B_4C and two La/B_4C multilayers. Three methods were used to analyze the reflectivity curves. As can be seen from Fig. 1 and Table 1, by using not only the corrected Bragg equation calculation but also the Fourier transform method, the periodic thickness is very accurate because almost no assumptions were introduced into the calculation. The curve-fitting method provides more comprehensive structure information but a more reasonable initial structure model is necessary. This model was based on the pre-analyses of the two methods mentioned above in this paper or even the fabrication goals.

The interface situations are different for different metal choice. In general the interfacial width of the metal-on-B_4C interface is smaller than that of the B_4C-on-metal interface. The metal-on-B_4C interfaces are produced by the impact of high-energy metal atoms on the B_4C surface during deposition. An exception is La/B_4C multilayers because lanthanum may be more chemically active and has a larger atom size. The B_4C-on-metal interface mainly embodies the characteristics of
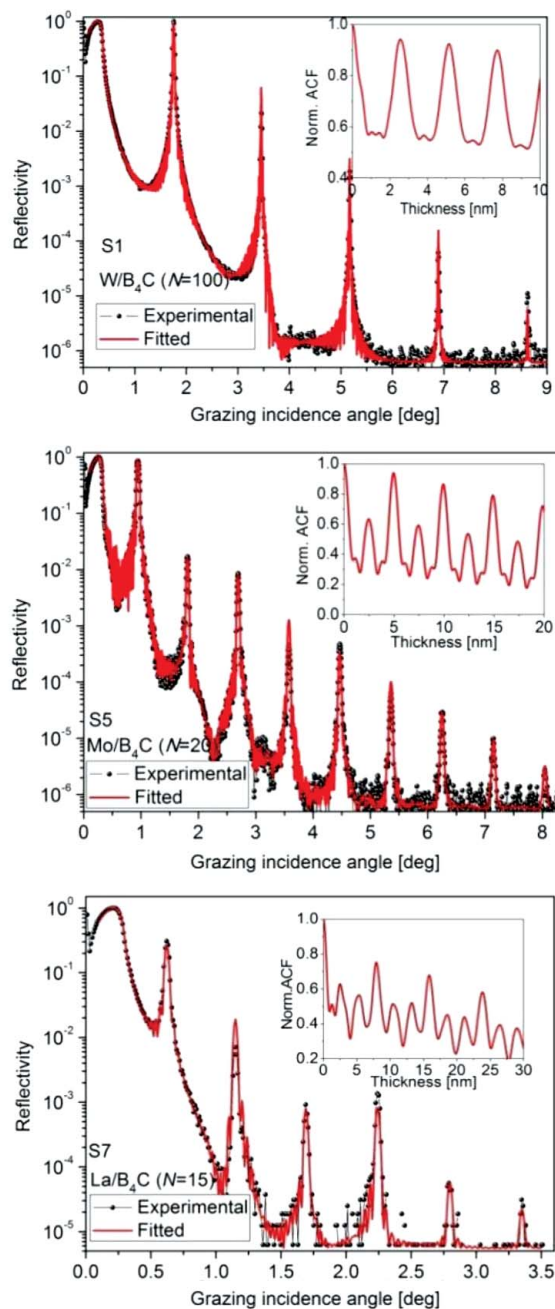
Figure 1
X-ray grazing-incidence reflectivity and fitted curve for the W/B₄C [sample 1, (a)], Mo/B₄C [sample 5, (b)] and La/B₄C [sample 7, (c)] multilayers. In the upper right-hand corner of each figure the normalized ACF curve is presented to show the layer thickness directly.

a rougher metal surface, and smaller boron and carbon atoms enable them to diffuse to the metal layer so that the B_4C-on-metal interlayer becomes thicker, normally beyond 0.4 nm. Comparing various multilayers, the W/B_4C multilayer has the best interface characteristics and La/B_4C has the worst, and can be compared with previous records (Andreev *et al.*, 2010). Keissig fringes disappear in the reflectivity curve of the La/B_4C multilayers because long-range disorder of the large interfacial width (Jiang *et al.*, 2011a) degrades the whole periodicity. High-angle reflectivity was measured as well.
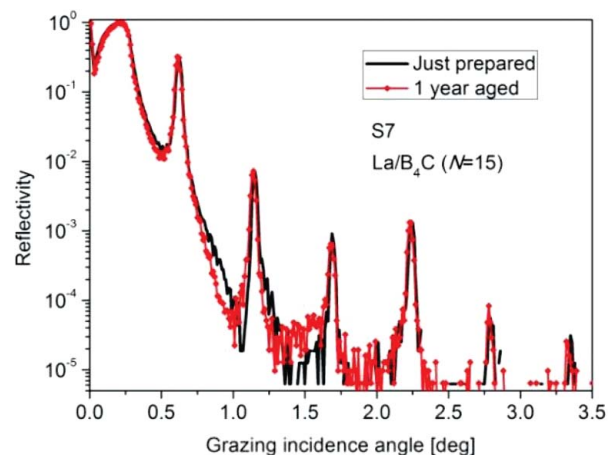

Figure 2
Grazing-incidence reflectivity curves for the La/B₄C multilayer (sample 7), just-prepared and after one year of storage.

Apart from ultrathin-period W/B_4C multilayers, slight crystallizations were found in other multilayers including the Mo(110), La(100) and Cr(110) crystallographic planes. It is clear that the deposition environments of these multilayers were not the same in this paper and changes of environments may produce slightly different multilayer performances.

As a consumable optics, multilayer structures are not always stable. Aging effects related to the inherent characteristics of the materials deserve to be studied. Three multilayer samples, W/B_4C, Mo/B_4C and La/B_4C (Fig. 2), were measured just-prepared and after long-time storage in a dry atmosphere environment (296 K). As can be seen from Table 2, the periodic thickness increased by 0.38% for the La/B_4C multilayer and by 0.24% for the Mo/B_4C multilayer after one year, but decreased by 0.05% for the W/B_4C multilayer after two years. The changes may result from interdiffusion mechanisms and stress release. Surface oxidation increased the stress and the changes of the layer thickness balanced the whole stress of the multilayer. The outermost layer thickness increases apparently by over 10% for the La/B_4C and Mo/B_4C multilayers because lanthanum and molybdenum have stronger oxidation capabilities than tungsten so that oxygen atoms penetrate through the B_4C layer gradually and react with metal atoms. The surface B_4C layer was also determined to absorb oxygen (Jiang *et al.*, 2011b). Thus it is important to deposit a stable capping layer to protect the multilayer structure.

The reciprocal-space map shown in Fig. 3 presents comprehensive scattering information for the Mo/B_4C multi-layer (sample 6). The first five Bragg maxima were determined. Along their lateral directions, clear and narrow crescent-shaped fringes can be seen owing to a good replication of the periodicity and roughness. Near the critical reflection area, the strong scattering signal means that the surface structure was oxide and sparse but did not influence the inner periodicity.

Three metal/B_4C multilayers were chosen to measure the X-ray diffuse scattering. In order to improve the precision of the analysis, rocking curve scans near different Bragg maximums were simultaneously fit based on equation (3), as shown

Table 1
Results of different structure characterizations for nine metal/B_4C multilayers.

A slash (/) means the value is lower than the resolution of this method.

No.	Material	Period number	Bragg equation Periodic thickness D (nm)	Fourier method Periodic thickness D (nm)	Layer thickness d (nm)	Curve fitting Layer thickness d (nm)	Interfacial width σ (nm)	Density ρ (% bulk)
S1	W	100	2.57 ± 0.01	2.56	/	0.92 ± 0.06	0.47 ± 0.09	95.29 ± 5.29
	B_4C				/	1.68 ± 0.06	0.22 ± 0.01	95.47 ± 18.1
S2	W	40	3.84 ± 0.01	3.84	1.67	1.68 ± 0.04	0.43 ± 0.06	95.60 ± 1.54
	B_4C				2.13	2.15 ± 0.04	0.21 ± 0.01	90.25 ± 13.54
S3	W	100	2.55 ± 0.01	2.55	/	1.00 ± 0.03	0.42 ± 0.04	84.67 ± 2.53
	B_4C				/	1.55 ± 0.03	0.24 ± 0.01	93.40 ± 12.84
S4	Mo	10	9.24 ± 0.01	9.25	4.94	4.84 ± 0.02	0.58 ± 0.02	95.96 ± 1.39
	B_4C				4.18	4.37 ± 0.02	0.26 ± 0.01	118.17 ± 5.05
S5	Mo	20	4.96 ± 0.01	4.96	2.18	2.22 ± 0.03	0.44 ± 0.02	97.85 ± 2.83
	B_4C				2.73	2.75 ± 0.03	0.18 ± 0.01	93.10 ± 7.93
S6	Mo	30	10.48 ± 0.02	10.49	4.43	4.42 ± 0.02	0.44 ± 0.02	96.67 ± 1.90
	B_4C				6.05	6.06 ± 0.02	0.23 ± 0.01	90.40 ± 4.87
S7	La	15	7.95 ± 0.01	7.93	5.11	5.00 ± 0.02	0.47 ± 0.03	83.79 ± 1.38
	B_4C				2.82	2.93 ± 0.02	0.33 ± 0.01	107.03 ± 3.32
S8	La	20	9.42 ± 0.03	9.38	/	7.66 ± 0.19	0.85 ± 0.12	99.46 ± 1.73
	B_4C				/	1.75 ± 0.19	0.46 ± 0.05	103.15 ± 17.91

Table 2
Change of the structure parameters after aging, for three metal/B_4C multilayers.

Sample	Status	Metal d (nm)	σ (nm)	ρ (% bulk)	B_4C d (nm)	σ (nm)	ρ (% bulk)	Surface B_4C d (nm)	σ (nm)	ρ (% bulk)
W/B_4C	Just prepared	1.94 ± 0.03	0.32 ± 0.07	90.42 ± 3.01	2.23 ± 0.04	0.31 ± 0.01	82.91 ± 11.7	2.66 ± 0.04	0.20 ± 0.01	114.7 ± 13.1
$N = 20$	Aged 2 years	1.93 ± 0.03	0.32 ± 0.07	93.70 ± 3.45	2.23 ± 0.04	0.31 ± 0.01	82.62 ± 12.4	2.61 ± 0.05	0.21 ± 0.01	117.8 ± 12.9
(S9)										
Mo/B_4C	Just prepared	2.30 ± 0.02	0.51 ± 0.02	91.30 ± 1.85	2.65 ± 0.03	0.20 ± 0.01	75.23 ± 9.12	3.10 ± 0.04	0.44 ± 0.03	89.21 ± 1.79
$N = 20$	Aged 1 year	2.30 ± 0.02	0.49 ± 0.02	98.70 ± 2.21	2.66 ± 0.03	0.18 ± 0.01	76.90 ± 8.79	3.33 ± 0.04	0.58 ± 0.04	85.87 ± 2.03
(S10)										
La/B_4C	Just prepared	5.00 ± 0.02	0.47 ± 0.03	83.81 ± 1.38	2.93 ± 0.02	0.33 ± 0.01	107.02 ± 3.32	4.53 ± 0.02	0.20 ± 0.02	109.76 ± 5.19
$N = 15$	Aged 1 year	5.01 ± 0.02	0.38 ± 0.02	82.83 ± 1.14	2.95 ± 0.02	0.33 ± 0.01	105.62 ± 2.98	5.08 ± 0.04	0.21 ± 0.02	90.67 ± 5.93
(S7)										

in Fig. 4. According to the fitted interfacial roughness σ_r and the interfacial width σ obtained by X-ray reflectivity measurement, the interdiffusion σ_d can be calculated by the equation $\sigma_d^2 = \sigma^2 - \sigma_r^2$. As can be seen from Table 3, the RMS

Figure 3
Logarithmic reciprocal-space mapping at grazing incidence for the Mo/B_4C multilayer ($N = 30$) (sample 6). The dark area is unavailable in the scan measurement. The tilted fringe is the reflectivity measurement and lateral fringes are rocking curve scans.

roughnesses for the three multilayers are almost the same but the Mo/B_4C and La/B_4C multilayers have larger interdiffusions. Comparing the lateral correlation length $\xi_\parallel$ and fractal exponent h, the Mo/B_4C and La/B_4C multilayers have a stronger lateral correlation and more apparent island growth features than the W/B_4C multilayer. Owing to the weak interdiffusion and small layer thickness, the vertical correlation length in the W/B_4C multilayer is over 100 times the periodic thickness. In contrast, the replication capability is very weak for La/B_4C multilayers. The vertical correlation length is only about four times the periodic thickness. The fractal model (Sinha *et al.*, 1988) was also used to fit the two-dimensional power spectral density curve calculated from various atomic force microscopy measurements (Bioscope BS2-Z, 256 × 256 pixels) of the W/B_4C multilayer (S11) at different scan scales from 10 µm × 10 µm to 0.5 µm × 0.5 µm. The result shows that the RMS roughness is 0.31 nm, the lateral correlation length is 63.63 nm and the fractal exponent is 0.06. The result is comparable with the characterization by X-ray diffuse scattering.

All measurements and relevant analyses mentioned above are suitable for all multilayer structures. The characteristics of the metal/B_4C multilayer structures (metal = W, Mo, La, Cr, Pt, Ni, Ti, Ru, Pd, *etc.*) can be extended to other typical
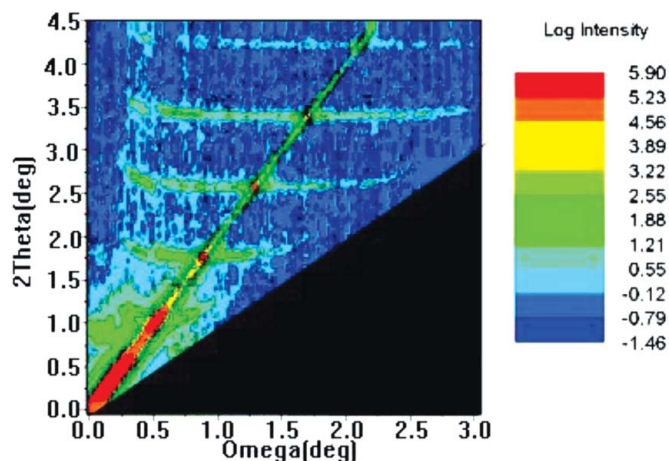
Table 3
Characterization results of different metal/B_4C multilayers using the X-ray diffuse scattering technique.

Sample	d (nm)	ρ (% bulk)	σ_r (nm)	σ_d (nm)	$\xi_{\parallel}$ (nm)	h	$\xi_{\perp}$ (nm)
W/B_4C $N = 20$ (S11)	0.83 ± 0.03	82.10 ± 2.72	0.29 ± 0.06	0.10 ± 0.06	17.19 ± 0.99	0.10 ± 0.01	286.64 ± 22.21
	1.53 ± 0.03	93.17 ± 5.81	0.17 ± 0.06	0.15 ± 0.06	10.19 ± 1.31	0.24 ± 0.01	
Mo/B_4C $N = 30$ (S6)	4.42 ± 0.02	96.67 ± 1.90	0.30 ± 0.04	0.32 ± 0.04	439.34 ± 21.14	0.01 ± 0.01	125.25 ± 15.89
	6.06 ± 0.02	90.07 ± 4.87	0.14 ± 0.05	0.17 ± 0.05	65.86 ± 13.33	0.07 ± 0.01	
La/B_4C $N = 15$ (S7)	5.01 ± 0.02	82.81 ± 1.38	0.35 ± 0.06	0.32 ± 0.06	440.56 ± 25.19	0.01 ± 0.01	28.32 ± 13.21
	2.95 ± 0.02	105.63 ± 3.32	0.11 ± 0.04	0.31 ± 0.04	28.92 ± 14.10	0.30 ± 0.01	
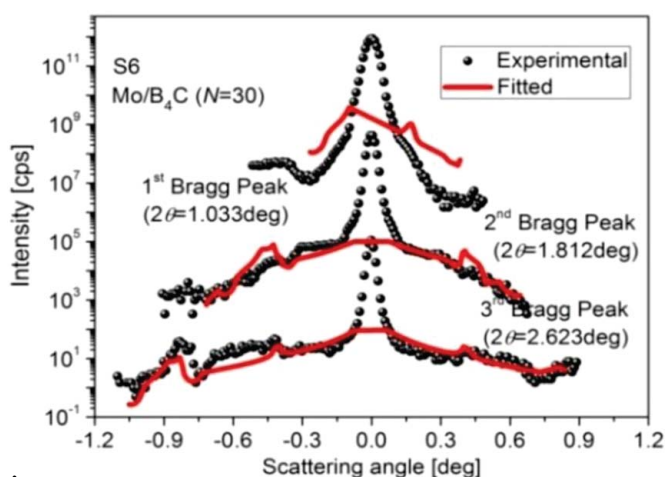
Figure 4
Rocking curve scans near three Bragg maxima and their fitted curves for the Mo/B_4C multilayer ($N = 30$) (sample 6).

material pairs such as B-based, C-based, Si-based and Y-based multilayers. The optical constants of the scattering layers (high-Z metal material) are the decisive factor regarding the reflectivity so that near bulk densities are required. Smooth and stable interfaces of the spacer layers (low-Z material) keep whole multilayers stable and further improve the optical performance. By the characterization of metal layers in this paper, other corresponding multilayer structures such as W/C, Mo/Si, Mo/Y and Mo/B_4C/Si/B_4C can be estimated. Accurate determination of the B_4C layers is also useful for more complicated characterization of multilayers which use B_4C as capping layers or barrier layers. Aging effects were also observed in this study. In the application, other environmental influences need to be considered as well. For example, heat load and surface contamination may be very serious problems when the multilayers are radiated by high-flux synchrotron X-rays. Related studies will be carried out in the future.

4. Conclusion

In order to study the properties of key B_4C-based multilayers, X-ray grazing-incidence reflectivity and diffuse scattering were used to characterize multilayer structures synthetically, including information of the thickness, density, interfacial roughness, interdiffusion, surface state, correlation length, *etc.* Corrected Bragg equation calculations, Fourier transform methods and curve fitting were combined to obtain accurate structure parameters, and the diffuse scattering technique distinguished interfacial roughness and interdiffusion well. The results show that the interfacial width of the metal-on-B_4C interface is about 0.2–0.3 nm, and that of the B_4C-on-metal is >0.4 nm. The interfaces in W/B_4C multilayers are sharpest, while the interfacial widths in La/B_4C multilayers are largest. Large interdiffusion occurs in the Mo/B_4C and La/B_4C multilayers, based on scattering measurements, while the interfaces in the W/B_4C multilayers are simple roughness states and have a smaller lateral and larger vertical correlation length. The main changes of the metal/B_4C multilayers aged in a dry atmosphere are surface oxidation and increase in period thickness. W/B_4C multilayers are stable enough so that no obvious oxidation appears at the surface and the period thickness keeps almost constant. All quantitative characterizations and comparisons will be useful to further improve the fabrication technology.

References

Andreev, S. S., Barysheva, M. M., Chkhalo, N. I., Gusev, S. A., Pestov, A. E., Polkovnikov, V. N., Rogachev, D. N., Salashchenko, N. N., Vainer, Yu. A. & Zuev, S. Yu. (2010). *Tech. Phys.* **55**, 1168–1174.
Bottger, T. C., Meyer, D., Paufler, P., Braun, S., Moss, M., Mai, H. & Beyer, E. (2003). *Thin Solid Films*, **444**, 165–173.
Bridou, F., Gautier, J., Delmote, F., Ravet, M.-F., Durand, O. & Modreanu, M. (2006). *Appl. Surf. Sci.* **253**, 12–16.
Gibaud, A. & Hazra, S. (2000). *Curr. Sci.* **78**, 1467–1477.
Gutman, G. (1994). *J. Xray Sci. Technol.* **4**, 142–150.
Holý, V., Kuběna, J., Ohlídal, I., Lischka, K. & Plotz, W. (1993). *Phys. Rev. B*, **47**, 15896–15903.
Jiang, H., Michette, A., Pfauntsch, S., Wang, Z., Zhu, J. & Li, D. (2011a). *Opt. Express*, **19**, 11815–11824.
Jiang, H., Zhu, J., Huang, Q., Xu, J., Wang, X., Wang, Z., Pfauntsch, S. & Michette, A. (2011b). *Appl. Surf. Sci.* **257**, 9946–9952.
Joensen, K., Gorenstein, P., Christensen, F. E., Gutman, G. & Wood, J. L. (1995). *Opt. Eng.* **34**, 283–288.
Mimura, H., Handa, S., Kimura, T., Yumoto, H., Yamakawa, D., Yokoyama, H., Matsuyama, S., Inagaki, K., Yamamura, K., Sano, Y., Tamasaku, K., Nishino, Y., Yabashi, M., Ishikawa, T. & Yamauchi, K. (2010). *Nat. Phys.* **6**, 122–125.
Pape, I., Hase, T. P. A., Tanner, B. K. & Wormington, M. (1998). *Physica B*, **253**, 278–289.
Parratt, L. (1954). *Phys. Rev.* **95**, 359–369.
Rack, A., Weitkamp, T., Riotte, M., Grigoriev, D., Rack, T., Helfen, L., Baumbach, T., Dietsch, R., Holz, T., Krämer, M., Siewert, F., Meduňa, M., Cloetens, P. & Ziegler, E. (2010). *J. Synchrotron Rad.* **17**, 496–510.
Sinha, S. K., Sirota, E. B., Garoff, S. & Stanley, H. B. (1988). *Phys. Rev. B*, **38**, 2297–2311.
Stepanov, S. A., Kondrashkina, E. A., Schmidbauer, M., Köhler, R., Pfeiffer, J.-U., Jach, T. & Souvorov, A. Yu. (1996). *Phys. Rev. B*, **54**, 8150–8162.

Stoev, K. & Sakurai, K. (1997). *Rigaku J.* **14**, 22–37.

Wang, H., Dhesi, S. S., Maccherozzi, F., Cavill, S., Shepherd, E., Yuan, F., Deshmukh, R., Scott, S., van der Laan, G. & Sawhney, K. J. (2011). *Rev. Sci. Instrum.* **82**, 123301.

Windt, D. L., Gullikson, E. M. & Walton, C. C. (2002). *Opt. Lett.* **27**, 2212–2214.

Wormington, M., Panaccione, C., Matney, K. M. M. & Bowen, D. K. (1999). *Philos. Trans. R. Soc. London A*, **357**, 2827–2848.